

# Multiwavelength study of the radio emission from a tight galaxy pair Arp 143

B. Nikiel-Wroczyński<sup>\*</sup>, M. Jamrozy, M. Soida, and M. Urbanik

*Astronomical Observatory, Jagiellonian University, ul. Orła 171, Kraków PL 30-244, Poland*

Accepted xxxx. Received xxxx; in original form xxxx

## ABSTRACT

We present results of the recent low-frequency radio observations of a tight galaxy pair Arp 143 at 234 and 612 MHz. These data are analysed together with the archive data at 1490, 4860, 8440, and 14940 MHz. From the analysis of the radio emission we derive constraints on the age of the radio emitting structures as well as on the properties of their magnetic field. We show that the collisional ring of NGC 2445 hosts strong magnetic fields (reaching  $12 \mu\text{G}$  in its northwestern part) manifesting as a steep-spectrum, nonthermal radiation at radio frequencies. The spectral age of this structure is higher than estimates derived for the star-forming regions from the  $\text{H}\alpha$  distribution, suggesting that the radio emission might have a different origin. The galactic core is of a very young spectral age, suggesting an ongoing starburst activity. Additionally we identify a possible ridge of emission between the ring galaxy and its elliptical companion NGC 2444.

**Key words:** galaxies: magnetic fields – galaxies: individual: NGC 2444, NGC 2445 – galaxies: pairs: individual: Arp 143 – galaxies: interactions – intergalactic medium – radio continuum: galaxies

## 1 INTRODUCTION

Collisional ring galaxies are scarce, yet very interesting objects. Their most prominent feature is the lack of a typical spiral structure, replaced by a narrow, ring-shaped accumulation of gas and stars. Such a peculiar distribution of matter is believed to form during collision of a spiral, gas-rich galaxy with a small, early type one (Lynds & Toomre 1976; Theys & Spiegel 1977). Galaxy pair consisting of NGC 2444 and 2445 is one of the few systems of ring galaxies that have been included in the Arp's Catalogue, denoted Arp 143 (Arp 1966). However, it differs significantly from the usual image of a ring system, as the ring structure in NGC 2445 is distorted, similar in appearance to a trapezoid with rounded vertices. The whole visible structure is dominated by local maxima of optical emission that are regions of intensive star formation (Burbridge & Burbridge 1959; Appleton et al. 1987, 1992). All of them are relatively young, and the central region is suspected to be undergoing starburst activity (Appleton et al. 1992). Moreover, the pair is known to be “trailing smoke”, as the  $\text{H I}$  morphology (Appleton et al. 1987) reveals a 150 kpc long tail of the neutral gas emission extending towards north. All this is suggestive for a collision of NGC 2445 with a compact

galaxy – possibly its companion, NGC 2444 (Appleton et al. 1992; Beirão et al. 2009). This collision disrupted the spiral disk and resulted in morphological distortions as well as in intensification of the star formation in particular regions of the collisional ring.

Not much is known about the radio emission from Arp 143. In fact, the only work that aimed at revealing the morphology of the radio-emitting medium of this object was that of Burke & Miller (1973), who used the Westerbork Synthesis Radio Telescope to study several interacting galaxies. These authors identified a source of radio emission within NGC 2445, associating it with one of the  $\text{H II}$  regions. However, they excluded the possibility of a purely thermal origin of the emission, as the luminosity was far too high to be caused by thermal processes only. Apart from that paper, the only available radio data was that from large surveys (e.g. Sulentic 1976 or Davis & Seaquist 1983). Appleton & Struck-Marcell (1996) mention a study of Arp 143 (as well as of ten other ring systems) made with the Very Large Array (VLA) at the frequency of 8440 MHz, but no detailed information is provided. Using Arp 10 as an example, these Authors suggest that the spectral index of the emission from ring galaxies might steepen inwards from the ring. Such phenomenon could be a result of a change from thermal to non-thermal emission and/or of ageing of

<sup>\*</sup> E-mail: iwan@oa.uj.edu.pl

the highest energy electrons, which leads to their absence in the inner region of the ring. However, almost nothing is known about the magnetic field and its properties. Also, cross-identifications between radio-emitting structures and their counterparts in other domains of the electromagnetic spectrum have not yet been made.

In this paper we present results from our recent observing project at the Giant Metrewave Radio Telescope (GMRT), in which Arp 143 has been studied at 234 and 612 MHz. The new observations are analysed together with the previously unpublished, archive VLA data at 1490, 4860, 8440, and 14940 MHz to produce high resolution maps of the radio emission and to study the magnetic field of this galaxy pair.

## 2 OBSERVATIONS AND DATA REDUCTION

### 2.1 GMRT data

The GMRT near Pune, India was used to observe Arp 143 at 234 and 612 MHz. The observations were carried out in a dual frequency mode as a part of our project “Magnetic field and galaxy interactions – from loose groups to mergers” (project code 23.025). The observations were carried out in February, 2013. The total observing time was 8 h and the bandwidths were 16 and 32 MHz at 234 and 612 MHz, respectively. The (u,v) data were reduced using the Astronomical Image Processing System (AIPS), including calibration and RFI-flagging. After obtaining initial images at both frequencies, they were processed by a self-calibration pipeline in order to correct the phase information. The final images have been (u,v)-tapered to obtain circular beams and then corrected for the primary beam shape. Two images have been made: one with resolution of 16 arcsec at 234 MHz, and another at 612 MHz, with resolution of 10 arcsec. Original beam sizes and noise levels of these maps can be found in Table 1.

### 2.2 Archive VLA data

In order to construct the radio continuum spectrum, and to derive the spectral age as well as to provide the magnetic field strength estimates for Arp 143, we searched through the archive of the VLA of the National Radio Astronomy Observatory (NRAO)<sup>1</sup>. We have obtained archived data at 1490, 4860, 8440, and 14940 MHz. Details on these observations can be found in Table 1. All these sets were calibrated, flagged and imaged using the AIPS. The 4860 MHz data allowed to run self-calibration. Except for the highest frequency, all the data sets were (u,v)-tapered to obtain a circular beam of 10″. The 14940 MHz image has not been tapered, as it was intended to be used only to derive the size of the galactic core of NGC 2445 and its flux. Additionally, the size of the primary beam at this frequency is nearly the same as the size of NGC 2445, resulting in non-reliable flux values besides the very center of this galaxy.

To include the calibration uncertainties, we have assumed a 5 per cent error for each integrated flux value for all the radio maps except the 234 MHz map, for which we adopt 8 per cent error.

## 3 RESULTS

Fig. 1 shows a composite RGB image built from *u*, *g*, *r* bands of the Sloan Digital Sky Survey (SDSS) data. An additional, H $\alpha$  component (map from Romano et al. 2008, taken from the NASA Extragalactic Database) was added to the red channel. Before merging, the H $\alpha$  map was rescaled to have signal values significantly higher than the median value of the *r* band emission in order to make the regions of molecular emission easily distinguishable. The colour image was then overlaid with the contours of radio emission at 612 MHz. Designations of different structures described in this paper – namely southern (S), northwestern (NW) and eastern (E) star-forming regions, intergalactic ridge and both galaxies – have also been marked. Measured fluxes of these structures are presented in Table 2.

The lowest frequency used in our study is 234 MHz and the map at this frequency is presented in Fig. 2a. It has the lowest resolution (circular beam of 16 arcseconds in diameter). The emission concentrates in the central-northern region of NGC 2445 and extends northwest, vanishing in the outer regions of NGC 2444 (which is otherwise a non-radio-emitting galaxy). The central part consists of the core and the NW region. Because of the beam size, the emission coming from these two entities is not separated. The radio emission coincides almost perfectly with the optically-emitting material in the northern part of the ring, but diminishes abruptly about 10 arcseconds south from the core of NGC 2445. Only an isolated patch of emission coincident with the southern star-forming region was detected. This is caused by the lower sensitivity to faint, extended structures at 234 MHz compared to 612 MHz.

The map at 612 MHz (Fig. 2b) has a modest resolution of 10 arcsec and a long integration time, resulting in a deep and detailed radio map. Despite higher resolution and frequency, this map shows more extended emission than that at 234 MHz. Apart from the core and the NW region, two other star-forming areas can be easily identified. Both in the eastern and the southern part of the ring, local maxima of the visible light distribution are coincident with peaks of the radio emission; the eastern structure is the weakest one. The northern extension that forms a ridge-like structure between NGC 2444 and NGC 2445 is also visible; it extends even further than that at 234 MHz, reaching NGC 2444.

The map at 1490 MHz (made from archive data) is presented in Fig. 2c. Short integration time and lack of the shortest baselines (due to the wide B-configuration of the VLA) resulted in the absence of most of the extended emission as well as in higher noise level. Only the core and the NW region are visible. There is no trace of emission from other parts of the collisional ring, nor from the aforementioned intergalactic ridge. It should be noted that the archive VLA data used in this study are of worse (u,v) coverage than the GMRT ones, resulting in lower detectability of the weak, extended emission. This mostly applies to the 1490

<sup>1</sup> NRAO is a facility of National Science Foundation operated under cooperative agreement by Associated Universities, Inc.

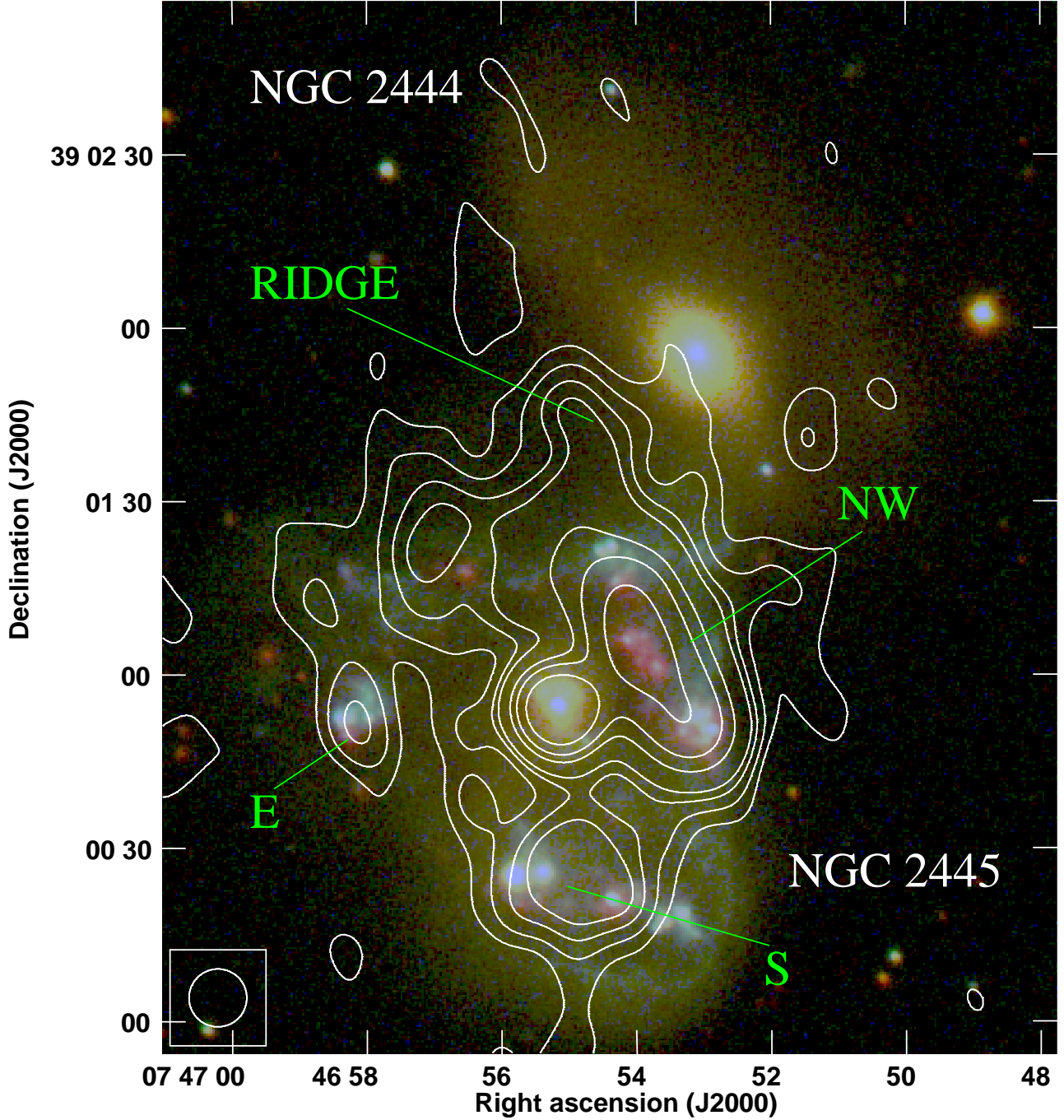
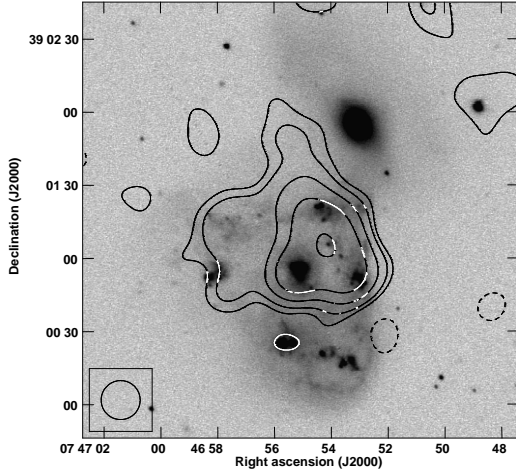


**Figure 1.** GMRT map of the TP emission from Arp 143 at 612 MHz overlaid upon an RGB image, with locations of the star-forming regions and intergalactic ridge indicated. The contour levels are 3, 5, 10, 20, 30, 50,  $100 \times 0.1$  mJy/beam (r.m.s. noise level). The angular resolution is 10 arcsec. The beam is represented by a circle in the lower left corner of the image. Details of the maps used to produce this RGB composite can be found in the text (Sect. 3).

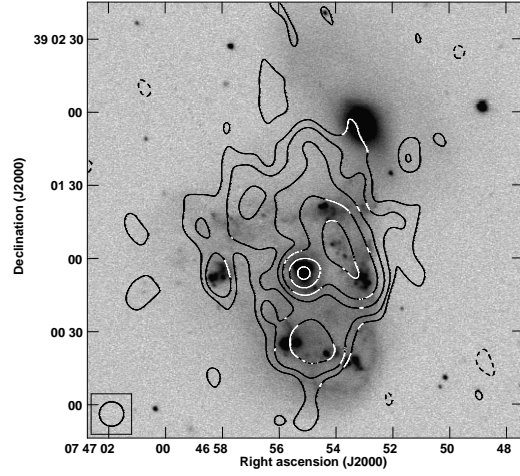
and 8440 MHz data, for which the  $(u,v)$  plane sampling is poor due to the integration times lower than 2 hours.

Considerably better  $(u,v)$  coverage and lack of strong RFI allowed to obtain a detailed map of the extended emission at 4860 MHz (Fig. 2d). Similarly to the 612 MHz map, not only the emission from the NW star formation region and the core can be seen, but the whole collisional ring is emitting at this frequency. From its structure one can dis-

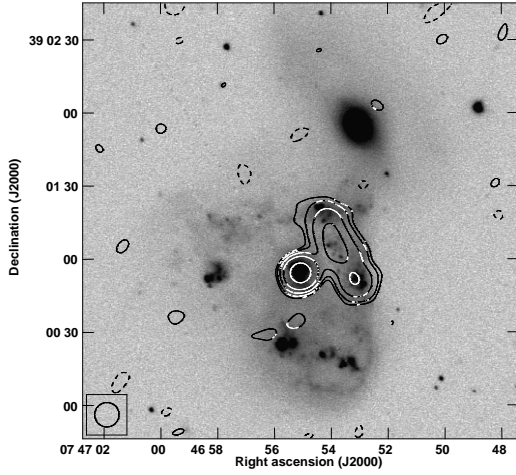
tinguish local maximum corresponding to the southern star forming region. Surprisingly, the eastern star forming region is indistinguishable from the extended emission. A patch of emission north from the ring, spatially coincident with the ridge detected both at 234 at 612 MHz is easily visible. It should be noted here that, unlike at 612 MHz, the inner part of the galaxy – an area between the ring and the core – is not visible in emission at 4860 MHz; this effect is more pro-



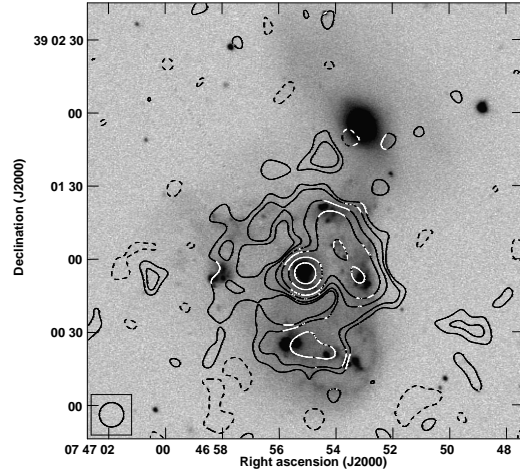
(a) GMRT map at 234 MHz. The r.m.s. noise level is 0.4 mJy/beam. The angular resolution is 16 arcsec.



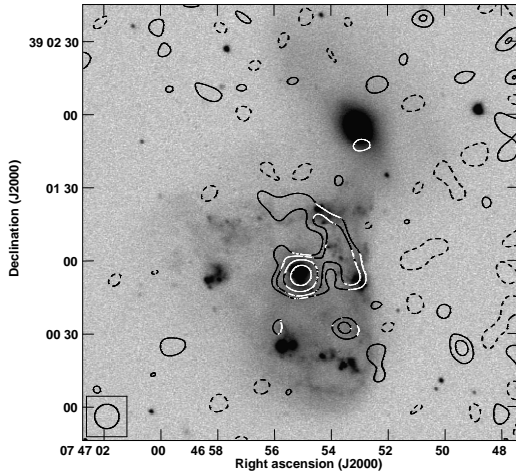
(b) GMRT map at 612 MHz. The r.m.s. noise level is 0.1 mJy/beam. The angular resolution is 10 arcsec.



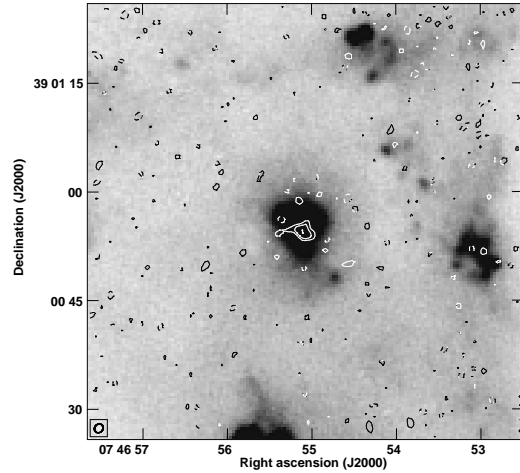
(c) VLA map at 1490 MHz. The r.m.s. noise level is 0.08 mJy/beam. The angular resolution is 10 arcsec.



(d) VLA map at 4860 MHz. The r.m.s. noise level is 0.02 mJy/beam. The angular resolution is 10 arcsec.



(e) VLA map at 8440 MHz. The r.m.s. noise level is 0.06 mJy/beam. The angular resolution is 10 arcsec.



(f) VLA map of the core at 14940 MHz. The r.m.s. noise level is 0.08 mJy/beam. The angular resolution is 1.28x1.13 arcsec.

**Figure 2.** Maps of the TP emission from Arp 143 at various frequencies overlaid upon an SDSS *g*-band image. The contour levels are  $-3$  (dashed),  $3, 5, 10, 20, 50, 100 \times$  r.m.s. noise level. The beam is represented by an ellipse in the lower left corner of the image.

**Table 1.** Basic information on the observational datasets used in this study

| Freq. [MHz] | Telescope | Proj. code | Date       | TOS [h] | Org. beam [arcsec] | Fin. beam [arcsec] | Noise [mJy/beam] |
|-------------|-----------|------------|------------|---------|--------------------|--------------------|------------------|
| 234         | GMRT      | 23_025     | 10.02.2013 | 8.0     | 14x11              | 16                 | 0.4              |
| 612         | GMRT      | 23_025     | 10.02.2013 | 8.0     | 7.5x5              | 10                 | 0.1              |
| 1490        | VLA B     | AD 182     | 05.09.1986 | 1.5     | 4x4                | 10                 | 0.08             |
| 4860        | VLA C     | AD 182     | 14.11.1986 | 2.7     | 4x4                | 10                 | 0.02             |
| 8440        | VLA D     | AA 146     | 25.08.1992 | 0.5     | 9x7                | 10                 | 0.06             |
| 14940       | VLA C     | AJ 105     | 29.05.1984 | 2.8     | 1.3x1.1            | 1.3x1.1            | 0.08             |

**Table 2.** Flux densities (with errors) obtained for the selected regions of radio emission. All values given in mJy. ND means no detection.

| Region | 234 MHz      | 612 MHz      | 1420 MHz    | 4860 MHz    | 8440 MHz    | 14960 MHz   |
|--------|--------------|--------------|-------------|-------------|-------------|-------------|
| Core   | 15.58 ± 1.40 | 11.14 ± 0.57 | 6.92 ± 0.36 | 3.59 ± 0.26 | 1.86 ± 0.11 | 0.81 ± 0.09 |
| NW     | 30.97 ± 2.61 | 20.07 ± 1.01 | 9.33 ± 0.49 | 3.24 ± 0.16 | 1.39 ± 0.12 | ND          |
| S      | ND           | 3.57 ± 0.25  | ND          | 0.57 ± 0.04 | ND          | ND          |
| E      | ND           | 0.66 ± 0.11  | ND          | 0.08 ± 0.02 | ND          | ND          |
| Ridge  | 3.30 ± 0.69  | 1.28 ± 0.10  | ND          | 0.16 ± 0.03 | ND          | ND          |

nounced in the spectral index map (Fig. 3), indicating a significantly steeper spectrum there.

At 8440 MHz the NW region is still visible, albeit significantly less prominent than at lower frequencies. Most of the extended emission has not been detected, because of the very short integration time of these archival data. Despite that, there is some minor extension of the NW region into the northern part of the collisional ring, but it barely exceeds the  $3\sigma$  level (Fig. 2e). Throughout the external parts of the image several isolated patches of noise-level radio emission, boosted by the primary beam correction are visible.

The primary beam of the observations at the highest frequency (14940 MHz) is very small, therefore only the very central part of NGC 2445 is visible. Only the core emerges from the noise (Fig. 2f). With the high resolution of this map, we can estimate the angular size of the radio-emitting region, which is approximately  $3 \times 2$  arcseconds (at the  $3\sigma$  level). This (assuming the distance estimate of  $54.9 \pm 3.8$  Mpc from de Vaucouleurs et al. 1991) yields the linear size of approximately 0.8 by 0.5 kpc. Similarly to the 8440 MHz image (Fig. 2e), loose patches of emission resulting from the primary beam correction are visible in the outer parts of the image.

Large primary beams in our low-frequency observations allowed us to search for the continuum counterpart of the giant HI tail extending north from the ring galaxy (Appleton et al. 1987). However, nothing was detected above the noise level in all the maps. Some remarks on the upper limit of the magnetic field strength in this area can be found in Sect. 4.2.

## 4 DISCUSSION

### 4.1 Spectral index

The spectral index map has been calculated between 612 and 4860 MHz and has a resolution of 10 arcsec. The input maps have been clipped at the  $5\sigma$  level to ensure that the noise

fluctuations would not be taken into account. The choice of this two maps – instead of the ones at the lowest and highest frequencies – was dictated by their resolution and quality. The 234 MHz map (Fig. 2a) has a rather low resolution of 16 arcsec, which does not allow to clearly distinguish different emitting regions. Moreover, despite large beamsize, it does not show larger extent of emission than the 612 MHz map. The 8440 MHz map (Fig. 2e) has a modest resolution of 10 arcsec, but it suffers from the short integration time, resulting in significant losses of the extended flux. This is not the case of the 4860 MHz map (Fig. 2d), which clearly shows the ring structure as well as a patch spatially connected to the intergalactic ridge. Therefore, the spectral index map – as well as all spectral index values used and presented in this study – have been calculated between the best-quality 612 and 4860 MHz maps. Throughout the paper we are using the  $S_\nu \propto \nu^{-\alpha}$  definition of the spectral index  $\alpha$ .

The emission from the core of NGC 2445 has a steeper spectrum (a mean spectral index of  $\approx 0.64 \pm 0.08$ ) than expected if it were a purely thermal source. This indicates that it has a synchrotron origin, as we would expect the thermal emission to manifest with a significantly flatter spectrum, which is not the case here (see Pacholczyk 1973 for details).

The spectrum of the star forming regions is steeper, with the mean spectral indices typical for an ageing population of relativistic electrons. The values for the particular regions are  $\alpha \approx 0.81 \pm 0.07$  for the northwestern,  $\alpha \approx 1.03 \pm 0.19$  for the eastern and  $\alpha \approx 0.89 \pm 0.06$  for the southern region. This means that the synchrotron emission dominates everywhere over the thermal component, even at the higher of these frequencies. This is not unusual; Niklas et al. (1997) have shown that the median thermal fraction at 1 GHz is  $0.08 \pm 0.01$ . The median non-thermal spectral index given by these authors is  $0.83 \pm 0.02$ , very close to the values derived for the star-forming regions in NGC 2445. This means domination of the high-energy, relativistic electrons supplied by the supernovae. Appleton & Struck-Marcell (1996) suggest that this process of electron supply would start some  $10^6$  years after the colli-

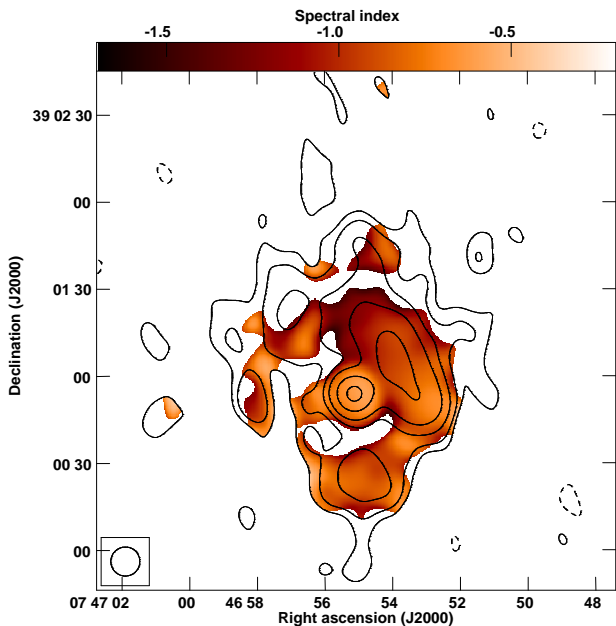


**Figure 3.** Map of the spectral index calculated between 612 and 4860 MHz with contours of the radio emission at 612 MHz overlaid. The contour levels are  $-3$  (dashed),  $3, 5, 10, 20, 30, 50 \times 0.02$  mJy/beam (r.m.s. noise level). The angular resolution is 10 arcsec.

sion. The estimated age of the density wave that gave birth to the NW region is  $\approx 85$  Myr (Beirão et al. 2009), indicating that such scenario is possible. The inner part of the ring has not been detected at 4860 MHz, indicating a very steep spectrum there. Assuming the 3-r.m.s. level as a constraint on the emission at 4860 MHz, we have estimated the spectral index to be  $> 1.8$  between 612 and 4860 MHz. Steepening of the spectral index inwards from the ring was mentioned by Appleton & Struck-Marcell (1996), who provided two possible explanations for such phenomenon: change from the mostly thermal to non-thermal radiation and/or ageing of the synchrotron electrons. Our findings suggest that in case of Arp 143 the second scenario is more probable.

The intergalactic ridge has a steep spectrum – characteristic for an ageing population of electrons – with a mean spectral index  $\alpha \approx 1.01 \pm 0.12$ . This is consistent with its identification as an intergalactic structure presented in Sect. 3. Also, it is steeper than that of the star-forming regions NW and S, suggesting a higher spectral age, as it is far away from the star-forming areas.

## 4.2 Magnetic field

Both the strength of the magnetic field  $B_{\text{TOT}}$  and its energy density  $E_B$  in the selected areas were calculated assuming the energy equipartition between the cosmic rays and the magnetic field, following the formulae presented in Beck & Krause (2005). We applied the BFELD code, which uses following parameters: total pathlength through the source  $D$ , proton-to-electron energy density ratio  $K_0$ , spectral index  $\alpha$ , and the mean synchrotron surface brightness of the chosen region to estimate its total field strength as well

as the magnetic energy density. The mean brightness has been obtained from the region’s integrated flux density  $S$  by dividing it by the square root of the number of the beams in the integration area.  $K_0$  was fixed as 100; such a value is suggested also for starburst galaxies (Lacki & Beck 2013). Values of all parameters used, together with the results of the estimation are presented in Table 3. The spectral index was calculated between the maps at 612 and 4860 MHz, which have the best quality. According to Niklas et al. (1997), thermal fraction at 1490 MHz for majority of galaxies does not exceed 10 per cent; even at 10000 MHz its mean value is about 25 per cent. This consistently yields thermal fraction at 4860 MHz significantly less than some 15–20 per cent. Except for the nucleus, a low thermal fraction is implied by steep radio spectra of discussed regions. Even in case of maximum value of 20 per cent, its neglecting leads to an overestimate of magnetic field strength by no more than 5–7 percent. Therefore, we decided not to take thermal emission into account.

For the NW part of the ring, we have used a pathlength of 5500 pc – derived from the angular size of the emitting region under an assumption of a cylindrical symmetry. The same size has been also adopted for all the other regions within the disk of NGC 2445 as well as for the ridge between it and NGC 2444. The estimated strength of the magnetic field in the NW region is therefore  $12.0 \pm 0.4 \mu\text{G}$ , and the energy density is  $5.8 \pm 0.5 \times 10^{-12} \text{ erg cm}^{-3}$ . This means that the magnetic field in this region is somewhat stronger than the average found in normal, spiral galaxies ( $9 \pm 1.3 \mu\text{G}$  – Niklas 1995). It is also comparable to that found in the shock region between the galaxies forming the Stephan’s Quintet ( $11.0 \pm 2.2 \mu\text{G}$  – Nikiel-Wroczyński et al. 2013). Values derived for the other star-forming regions are very similar (see Table 3).

Estimates for the intergalactic ridge do not differ much from that for the star-forming regions. As its spectrum is steeper than that of the star-forming regions (except for the eastern region, which has a comparable  $\alpha$ ), the strength of the magnetic field is nearly the same despite lower surface brightness. For an intergalactic structure, value of  $\approx 9 \mu\text{G}$  is a rather high strength. There is no clear counterpart to this entity in any other spectral domain. Most possibly, the magnetic field – enhanced in the star-forming NW region – is dragged with the intergalactic gas during the tidal interaction with the companion galaxy. Such a structure can result from a partially ordered B-field, dragged and stretched during the interaction. The total magnetic field is, in terms of its strength and energy density, similar to that of the iconic colliding pair of galaxies, the Taffies (Condon et al. 1993). Unfortunately, the setup of the low-frequency observations (simultaneous dual-frequency mode 234/612 MHz) did not allow to perform full Stokes observations, and we have not detected polarisation in any of the VLA datasets. Polarisation data is necessary to confirm or reject this scenario.

As the core of the collisional ring galaxy exhibits a spectrum that suggests a non-thermal origin of the emission ( $\alpha \approx 0.64 \pm 0.08$ ), we derived estimates for the magnetic field of the core, too. We used a pathlength of 650 pc – a mean of its linear dimensions (see Sect. 3). The resulting field is strong, as it reaches  $38.8 \pm 1.7 \mu\text{G}$ . Its energy density is equal to  $6.0 \pm 0.5 \times 10^{-11} \text{ erg cm}^{-3}$ . The core is supposed to undergo starburst activity (Appleton et al. 1992), and for

**Table 3.** Parameters used for the estimation of the magnetic field properties and resulting values

| Region | $D$ [kpc]       | $\alpha$        | $S_{4.86}$ [mJy] | $B_{\text{TOT}}$ [ $\mu\text{G}$ ] | $E_B$ [ $\text{erg cm}^{-3}$ ] |
|--------|-----------------|-----------------|------------------|------------------------------------|--------------------------------|
| Core   | $0.65 \pm 0.15$ | $0.64 \pm 0.08$ | $3.24 \pm 0.16$  | $38.8 \pm 1.7$                     | $60 \pm 5 \times 10^{-12}$     |
| NW     | $5.5 \pm 0.5$   | $0.81 \pm 0.07$ | $3.59 \pm 0.13$  | $12.0 \pm 0.4$                     | $5.8 \pm 0.5 \times 10^{-12}$  |
| S      | $5.5 \pm 0.5$   | $0.89 \pm 0.06$ | $0.57 \pm 0.04$  | $9.9 \pm 0.3$                      | $3.9 \pm 0.3 \times 10^{-12}$  |
| E      | $5.5 \pm 0.5$   | $1.03 \pm 0.19$ | $0.08 \pm 0.02$  | $8.7 \pm 0.6$                      | $3.0 \pm 0.4 \times 10^{-12}$  |
| Ridge  | $5.5 \pm 0.5$   | $1.01 \pm 0.12$ | $0.16 \pm 0.03$  | $9.2 \pm 0.6$                      | $3.3 \pm 0.3 \times 10^{-12}$  |

a compact region of efficient electron supply such a number is not surprising.

The radio continuum counterpart for the tidal tail has not been detected, but we could obtain the upper limit for the magnetic field strength and energy in its area. We have assumed that the tail has a cylindrical symmetry with a diameter of 20 kpc (Appleton et al. 1987) and a steep spectral index of 1.0. Once again, we used the BFELD code, calculating the magnetic field strength using information at 234, 612 and 4860 MHz. The upper limit for the strength was estimated as  $< 4.6 \mu\text{G}$ . The corresponding limit for the magnetic field energy is  $< 1.1 \times 10^{-12} \text{erg cm}^{-3}$ . However, these values are of high uncertainty, as the estimates of the tail parameters are rather rough. Assuming the radio-emitting medium to be more shallow (which is possible, as there are hints of narrowing in certain regions of the tail), the limit for the magnetic field strength would rise up – to approximately  $8.5\text{--}12 \mu\text{G}$  (in case of the depth of 5 and 1 kpc, respectively) and its energy density would reach  $2.8 - 6.3 \times 10^{-12} \text{erg cm}^{-3}$ . This indicates that a relatively strong magnetic field could remain undetected.

### 4.3 Age of the structures

Good frequency coverage allows to estimate the spectral age of the core and the NW region. The amount of time elapsed since the last acceleration of the particles in a given structure can be calculated under assumption that the observed steepening of the radio spectrum is caused by the synchrotron and/or inverse-Compton processes. We decided to use the SYNAGE package (Murgia 1996), which has an implementation of the Jaffe–Perola (Jaffe & Perola 1973, JP), Kardashev–Pacholczyk (Kardashev 1963; Pacholczyk 1973, KP), and continuous injection (Pacholczyk 1973; Myers & Spangler 1985; Carilli et al. 1991, CI) models of electron energy losses. The JP model assumes that the particles get isotropised in the pitch angle with the time-scale of isotropisation much smaller than the radiative lifetime. The KP model assumes that each electron maintains its original pitch angle. The CI model includes the continuous injection of a power-law distributions of relativistic electrons. The observed spectrum in this case is the sum of the emission from the various electron populations at different synchrotron ages, ranging from zero to the age of the source. The flux density at frequencies below the synchrotron break rises with time, since new particles are being added. All these models assume a constant magnetic field. SYNAGE uses the flux values at different wavelengths (spectral energy distribution, SED) to determine the spectral index

of the injected electron population  $\alpha_{\text{inj}}$ , and the spectral break frequency  $\nu_{\text{break}}$  (frequency above which the observed spectrum steepens from the initial one, in GHz). Using the magnetic field strength determined in Sect 4.2, now expressed in nT, the spectral age can be calculated as:

$$\tau = 50.3 \frac{B^{1/2}}{B^2 + B_{\text{IC}}^2} \times (\nu_{\text{break}}(1+z))^{-1/2} [\text{Myr}] \quad (1)$$

where  $B_{\text{IC}} = 0.338(1+z)^2$  is the CMB magnetic field equivalent (Alexander & Leahy 1987). Estimated values of the injection spectral index  $\alpha_{\text{inj}}$ , break frequency  $\nu_{\text{break}}$ , and the spectral age are summarised in Table 4.

Both standard JP and KP models give a good representation of the data, but the fit derived using the JP model is slightly better (judging on the  $\chi^2$  value – see Fig. 4). The fit given by the CI model is worse, as the goodness-of-fit parameter  $\chi^2$  is of an order of magnitude higher than for JP and KP. No matter the chosen model, it is clearly visible that the spectral age of the core is very low, ranging from 1.6 to 5.2 Myrs. Bearing in mind the possible starburst occurrence (Appleton et al. 1992) this is a reasonable value; starburst activity would result in an efficient supply of young electrons, producing a flat spectrum. The derived spectral index of the injected electron population (significantly below 0.5 for JP and KP, and  $0.46 \pm 0.05$  for CI) indeed suggests a very flat, albeit still reliable spectrum; Weiler & Sramek (1988) give  $\alpha = 0.3$  as the flattest spectrum available for the supernova remnants (SNR), and supernovae are the main sources of the non-thermal emitting electrons in the star-forming galaxies. Moreover, Hummel (1991) lists several galaxies for which the injection spectra have  $\alpha$  in range of 0.3–0.5, similar to our estimates, both for the core and the NW region.

The spectral fits for the NW region can be seen in Fig. 5. Similarly to the case of the core, the JP and KP fits give better representation than the CI model. The age estimates range from 9.0 to 39.1 Myrs. Even in case of the lowest value, the result is higher than the estimates of the age of the star-forming knots given by Beirão et al. (2009), who identifies two very young (2.5 and 3.5 Myrs) structures in the area coincident with our NW region. This means that the high energy electrons associated with the magnetic field are older than those involved in the recent star-forming processes. This is consistent with the steep, non-thermal spectrum of this area (Sect. 4.1). Most likely the magnetic field has been enhanced during the propagation of the density wave that formed the collisional ring (see Appleton & Struck-Marcell 1996), and the recent star-forming activity has weaker effect on its properties (e.g. flattens the spectrum, but as for it is a non-dominant component, the overall spectrum is still relatively steep). The injection spectral index of around 0.5



is reasonable for an extended region of synchrotron radio emission.

Finally, we note that the definite rejection of the CI model on the basis of available data may be premature. While for the core the mentioned fitted spectrum (Fig. 4) has generally an overmuch small curvature, for the NW region the CI model differs from the data and other fits only at the high and low ends of the analysed spectrum (Fig. 5). We keep in mind that the flux measurements at low frequencies may be affected by free-free absorption caused by ionised gas. This would decrease the flux at 234 MHz. At the high-frequency end of the radio spectrum, a small  $\lambda/D$  ratio and a short integration time (hence a poor (u,v) plane coverage) of interferometric observations may cause a substantial flux loss of faint extended emission. With the currently available data both effects cannot be evaluated quantitatively. We estimated possible effects of hypothetical free-free absorption and of loss of extended structures at lowest and highest frequencies, respectively upon the results of CI model fits. We performed an experiment by increasing arbitrarily the measured flux densities of the NW region at extreme frequencies by values needed to improve the  $\chi^2$  for the CI model. It turns out that achieving similar goodness-of-fit as for the JP and KP models for the NW region requires approximately 10 per cent higher flux at 234 MHz and 30 per cent higher flux at 8440 MHz. We found that the break frequency, and thus the age estimate (noted as NW-SIM in Table 4), appeared to be similar to those obtained from the original CI fit. In the light of these estimates and of the current data status we cannot simply reject the CI model. Though it implies (regardless possible flux losses) a substantially higher limits to the spectral age than JP and KP spectral fits, it should be still kept in mind as an acceptable solution for the NW region.

#### 4.4 Morphology of the radio emission distribution

As mentioned in Sect. 1, the collisional ring of NGC 2445 is far from being circular/elliptical. So is the radio emission distribution in this galaxy: its SE side is less prominent than the NW one (not only in the radio regime). The emission is weaker – not only at 234 MHz (Fig. 2a), but also in better quality maps at 612 (Fig. 2b) and 4860 MHz (Fig. 2d). Star-forming regions in the SE part have also somewhat weaker magnetic fields and are less extended. Additionally, the angular distance from the core to the ring is lower in the NW part than in the SE part. The asymmetry may result from an ongoing interaction with NGC 2444, resulting in the compression of the NW part of the ring, which leads to the amplification of the magnetic field. Such interaction has been suggested multiple times (e.g. Appleton et al. 1992, Beirão et al. 2009). The distribution of the radio-emitting medium is very similar to that of the molecular emission (Beirão et al. 2009), including lack of the PAH radio emission in the southernmost knot (labeled *D* in Beirão et al. 2009) and weak emission in the northernmost knot (*G* in Beirão et al. 2009). Both these knots have the lowest far-UV star-forming rates. This suggests that the radio emission deficiency might be result of faster CR diffusion when compared to the synchrotron losses. Weaker magnetic field – especially in the southern part – allows CR electrons to diffuse regardless of their energy.

In general, the overall radio distribution seems to confirm the scenario of an off-axis collision and later, on-going interaction with NGC 2444. The radio ring follows the distribution of the neutral and ionised gas (Higdon et al. 1997, Beirão et al. 2009), which is suspected to have formed as a result of such collision. The asymmetry of the emission together with the intergalactic ridge provides an evidence of an interaction with the companion galaxy. However, further details of the interaction history would need examination of the regular magnetic field properties, i.e. analysis of the polarisation data (like that was done for NGC 3627 by Soida et al. 2001, or the Virgo cluster spirals, by Weżgowiec et al. 2012),

## 5 CONCLUSIONS

We observed the tight galaxy pair Arp 143 with the GMRT at 234 and 612 MHz. Radio emission maps were analysed together with the archive VLA data at 1490, 4860, 8440, and 14940 MHz to study the spectral age of the features seen in the system, morphology of the radio emitting medium and the magnetic field strength and energy within the pair. The results obtained are summarised below:

- The radio emission from NGC 2445 concentrates in the northwestern part of the optical ring, extending to the outer parts of NGC 2444. Several distinct radio emitting regions can be identified: the core, three star-forming regions, and an intergalactic ridge.
- The galactic core is a not very compact (0.8 on 0.5 kpc), synchrotron-emitting source. It possesses a strong magnetic field of  $38.8 \pm 1.7 \mu\text{G}$ . It has a relatively flat spectrum ( $\alpha = 0.64 \pm 0.08$ ) and the age estimate yields 1.6 – 5.2 Myrs (depending on the model fitted). This is consistent with its identification as a starburst region.
- The northwestern region of radio emission, coincident with the star-forming knots, possesses magnetic field with strength of  $12.0 \pm 0.4 \mu\text{G}$  – somewhat stronger than the typical galactic fields. Its spectrum is typical for an ageing, yet not very old electron population, with a mean spectral index of  $0.81 \pm 0.07$ . The spectral age estimate of 9.0 – 39.1 Myrs is higher than that of the star-forming knots given by Beirão et al. (2009), indicating that most of the radio emission is associated with an older electron population, that was injected while a density wave was propagating through the intergalactic medium.
- Two other – southern and eastern – regions of star-formation have been detected. Their magnetic fields ( $9.9 \pm 0.3$  and  $8.7 \pm 0.6 \mu\text{G}$ , respectively) are somewhat weaker than that of the northwestern one.
- Distribution of the radio emission from NGC 2445 shows significant asymmetry, with the northwestern part being more luminous than the southeastern one. This supports the scenario of an ongoing interaction with NGC 2444.
- NGC 2444 is in general a non-radio-emitting galaxy, apart from the intergalactic radio ridge connecting it with NGC 2445. The magnetic field in the ridge is comparable to those found in the star-forming regions. It is also similar to that found in the intergalactic bridge of the Taffy galaxies (Condon et al. 1993).
- There are no signs of radio emission from the HI tail reported by Appleton et al. (1987). Depending on the – yet unknown – depth of the radio emitting medium, the upper



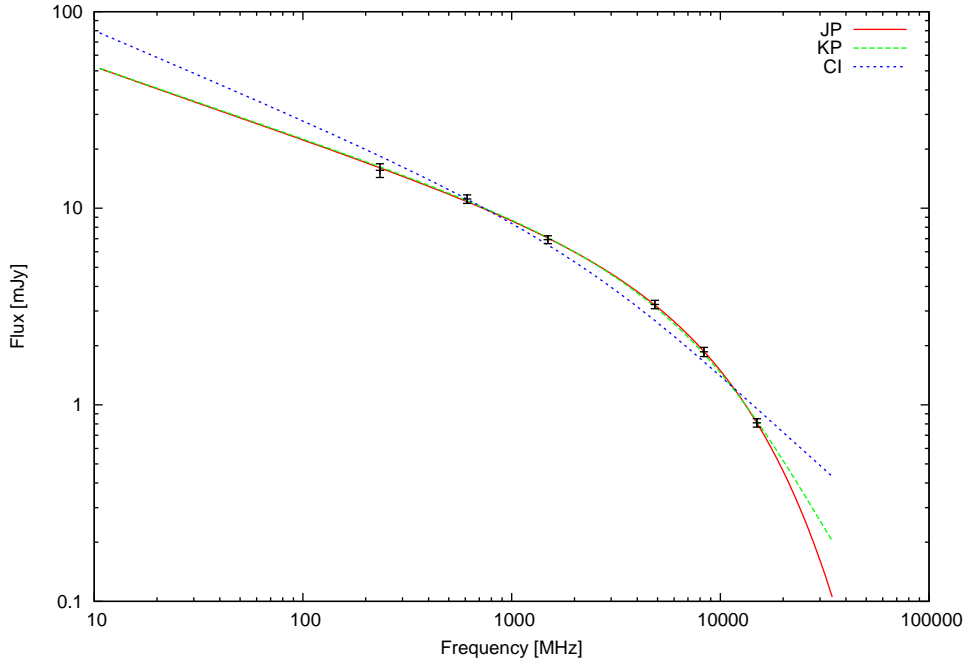


**Figure 4.** Three different models of the electron energy losses models fitted to the SED of the core of NGC 2445: Jaffe-Perola (JP – red), Kardashev-Pacholczyk (KP – green) and continuous injection (CI – blue). Details of the fitting scheme and characteristic fit parameters are provided in Sect. 4.3.

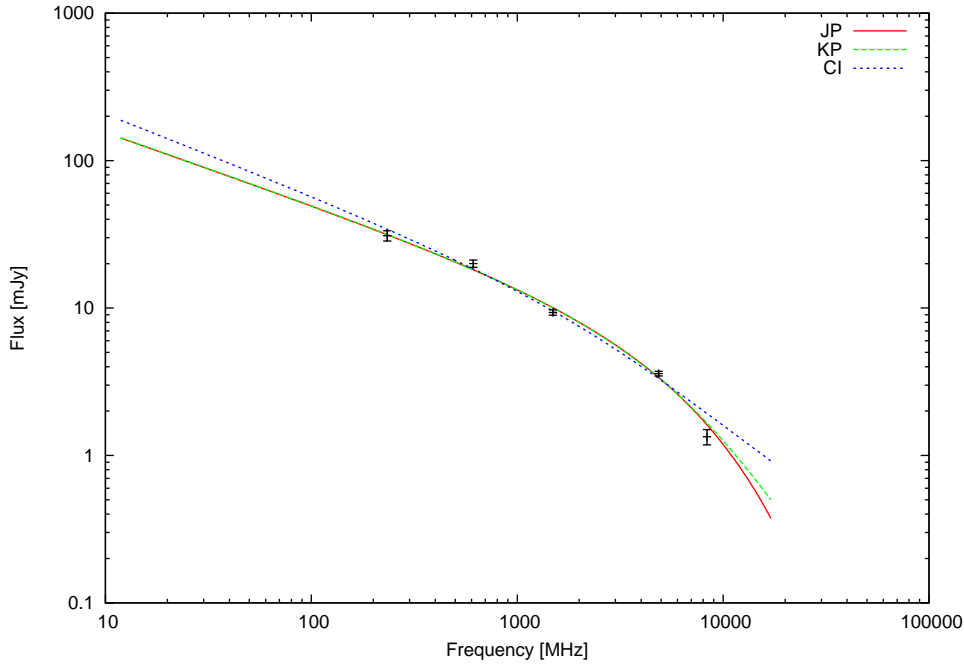


**Figure 5.** Three different models of the electron energy losses models fitted to the SED of the NW region of NGC 2445: Jaffe-Perola (JP – red), Kardashev-Pacholczyk (KP – green) and continuous injection (CI – blue). Details of the fitting scheme and characteristic fit parameter are provided in Sect. 4.3.

limit for the magnetic field in the tidal tail is  $< 4.5 - 12 \mu\text{G}$ , yielding  $< 1.1 - 6.3 \times 10^{-12} \text{erg cm}^{-3}$  for its energy density.

## ACKNOWLEDGEMENTS

We wish to thank the anonymous referee, whose comments and suggestions allowed us to significantly improve this article. We thank the staff of the GMRT that made these observations possible. GMRT is run by the National Cen-

**Table 4.** Parametres of the spectral fits

| Region | Model | $\chi^2$ | $\alpha_{\text{inj}}$  | $\nu_{\text{break}}[\text{GHz}]$ | Spectral age [Myrs] |
|--------|-------|----------|------------------------|----------------------------------|---------------------|
| Core   | JP    | 0.25     | $0.38^{+0.04}_{-0.01}$ | $12.1^{+2.7}_{-1.0}$             | 1.6 – 2.1           |
| Core   | KP    | 0.48     | $0.38^{+0.03}_{-0.01}$ | $6.2^{+1.3}_{-0.5}$              | 2.2 – 2.9           |
| Core   | CI    | 12.18    | $0.46 \pm 0.05$        | $2.8^{+1.6}_{-1.0}$              | 2.9 – 5.2           |
| NW     | JP    | 5.77     | $0.49 \pm 0.07$        | $9.3^{+4.8}_{-2.2}$              | 9.0 – 14.1          |
| NW     | KP    | 6.34     | $0.49^{+0.08}_{-0.07}$ | $5.0^{+3.2}_{-1.4}$              | 11.8 – 19.5         |
| NW     | CI    | 10.81    | $0.54^{+0.09}_{-0.10}$ | $2.3^{+2.7}_{-1.4}$              | 15.1 – 39.1         |
| NW-SIM | CI    | 2.77     | $0.52^{+0.11}_{-0.14}$ | $2.8^{+5.0}_{-2.4}$              | 12.1 – 58.6         |

tre for Radio Astrophysics of the Tata Institute of Fundamental Research. BNW is indebted to Eric Greisen, NRAO, for his help in preparing the RGB composite maps using the AIPS. This research has been supported by the scientific grant from the National Science Centre (NCN), dec. No. 2011/03/B/ST9/01859. This research has made use of the NASA/IPAC Extragalactic Database (NED) which is operated by the Jet Propulsion Laboratory, California Institute of Technology, under contract with the National Aeronautics and Space Administration. This research has made use of NASA's Astrophysics Data System. Funding for the SDSS and SDSS-II has been provided by the Alfred P. Sloan Foundation, the Participating Institutions, the National Science Foundation, the U.S. Department of Energy, the National Aeronautics and Space Administration, the Japanese Monbukagakusho, the Max Planck Society, and the Higher Education Funding Council for England. The SDSS Web Site is <http://www.sdss.org/>.

## REFERENCES

- Alexander P., Leahy J. P., 1987, MNRAS, 225, 1  
 Appleton P. N., Ghigo F. D., van Gorkom J. H., Schombert J. M., Struck-Marcell C., 1987, Nature, 330, 140  
 Appleton P. N., Schombert J. M., Robson E. I., 1992, ApJ, 385, 491  
 Appleton P. N., Struck-Marcell C., 1996, Fund. of Cosm. Phys., 16, 111  
 Arp H., 1966, ApJS, 14, 1  
 Beck R., Krause M., 2005, AN, 326, 414  
 Beirão P., Appleton P. N., Brandl B. R., Seibert M., Jarrett T., Houck J. R., 2009, ApJ, 693, 1650  
 Carilli C. L., Perley R. A., Dreher J. W., Leahy J. P., 1991, ApJ, 383, 554  
 Condon J. J., Helou G., Sanders D. B., Soifer B. T., 1993, ApJ, 105, 1730  
 Davis L. E., Seaquist E. R., 1983, ApJS, 53, 269  
 Burbidge E. M., Burbidge G. R., 1959, ApJ, 130, 12  
 Burke B. F., Miley G. K., 1973, A&A, 28, 379  
 de Vaucouleurs G., de Vaucouleurs A., Corwin H. G., Buta R. J., Paturel G., Fouque P. Third Reference Catalogue of Bright Galaxies (RC3). Springer-Verlag, New York, 1991  
 Jaffe W. J., Perola G. C., 1973, A&A, 26, 423  
 Higdon J. L., Rand, R. J., Lord, S. D., 1997, ApJ, 489, L133  
 Hummel E., 1991, A&A, 251, 442  
 Kardashev N. S., 1962, SvA, 6, 317  
 Lacki B., Beck R., 2013, MNRAS 430, 3171  
 Lynds R., Toomre A., 1976, ApJ, 209, 382  
 Murgia M., 1996, Laurea Thesis, University of Bologna  
 Myers S. T., Spangler S. R., 1985, ApJ, 291, 52  
 Nikiel-Wroczyński B., Soida M., Urbanik M., Beck R., Bommans D. J., 2013, MNRAS, 435, 149  
 Niklas S., 1995, PhD thesis, University of Bonn  
 Niklas S., Klein U., Wielebinski R., 1997, A&A, 322, 19  
 Pacholczyk A. G., Radio Astrophysics. Freeman, San Francisco, 1970, Mir, Moscow, 1973  
 Romano R., Mayya Y. D., Vorobyov E. I., 2008, AJ, 136, 1259  
 Soida M., Urbanik M., Beck R., Wielebinski R., Balkowski C., 2001, A&A, 378, 40  
 Sulentic J. W., 1976, ApJS, 32, 171  
 Theys J. C., Spiegel E. A., 1977, AJ, 212, 616  
 Weiler K. W., Sramek R. A., 1988, Ann. Rev. Afca, 26, 295  
 Weźgowiec M., Urbanik M., Beck R., Chyży K. T., Soida M., 2012, A&A, 545, 69